Enamel microstructure of permanent and deciduous teeth of a species of notoungulate *Toxodon*: Development, functional, and evolutionary implications

PATRÍCIA R. BRAUNN, JORGE FERIGOLO, and ANA M. RIBEIRO

Braunn, P.R., Ferigolo, J., and Ribeiro, A.M. 2021. Enamel microstructure of permanent and deciduous teeth of a species of notoungulate *Toxodon*: Development, functional, and evolutionary implications. *Acta Palaeontologica Polonica* 66 (2): 449–464.

Enamel microstructure is studied here in *Toxodon* sp., a notoungulate from the Pleistocene of South America. The material includes 13 specimens from outcrops in São Paulo and Rio Grande do Sul states, Brazil. Analyses of ground sections of upper and lower incisors, premolars, molars, and deciduous premolars by scanning electron microscopy reveal Schmelzmuster with three enamel types: modified radial enamel (MRE), associated with the enamel-dentine junction (EDJ); Hunter-Schreger bands (HSB), an intermediary layer with decussating prisms; and radial enamel (RE), a layer placed next to the outer enamel surface. Microstructural features vary in each tooth category, on the buccal and lingual sides, as well as in the different regions of each tooth. The proportion of RE increases in the occlusal area of I2, which commonly exhibits intense wear, and may be related to abrasion resistance. HSB thickness ranges from 6 to 20 prisms, with the thickest portions placed in areas with intense masticatory loads. The most concentrated packing densities of HSB in the upper incisors and lower premolars suggest these teeth bore the greatest biomechanical demands. Incisors and cheek teeth show differentiation of Schmelzmuster, suggesting dental antagonistic contact areas, as well as leading and trailing edges. Deciduous premolars exhibit enamel in the early stages of development, and a neonatal line is observed almost parallel to the EDJ, possibly related to biological stress during birth. The EDJ is scalloped in all dental categories, with varying sizes and shapes. Larger and more pronounced scallops are observed in I2, i3, p4, and in the enamel folds of the upper and lower cheek teeth, associated with microstructural features indicative of greater biomechanical demands. Microstructural enamel findings presented here corroborate morphological trends in the dentition of Notoungulata related to hypsodonty, providing greater resistance to the consumption of abrasive diets in these euhypsodont-toothed herbivores.

Key words: Mammalia, Toxodontidae, euhypsodont teeth, enamel-dentine junction, Hunter-Schreger bands, neonatal line, Pleistocene, Brazil.

Patrícia R. Braunn [pbraunn@gmail.com], Programa de Pós-Graduação em Geociências, Instituto de Geociências, Universidade Federal do Rio Grande do Sul, Av. Bento Gonçalves 9500, 91501-970, Porto Alegre, Brazil.
Jorge Ferigolo [jorge-ferigolo@sema.rs.gov.br], Seção de Paleontologia, Museu de Ciências Naturais, Secretaria do Meio Ambiente e Infraestrutura, Av. Dr. Salvador França, 1427, 90690-000, Porto Alegre, Brazil;
and Ana M. Ribeiro [ana-ribeiro@sema.rs.gov.br], Seção de Paleontologia, Museu de Ciências Naturais, Secretaria do Meio Ambiente e Infraestrutura, Av. Dr. Salvador França, 1427, 90690-000, Porto Alegre, Brazil; Programa de Pós-Graduação em Geociências, Instituto de Geociências, Universidade Federal do Rio Grande do Sul, Av. Bento Gonçalves 9500, 91501-970; Porto Alegre, Brazil.

Received 20 May 2020, accepted 20 October 2020, available online 7 June 2021.

Introduction

"How wonderfully are the different orders, at the present time so well separated, blended together in different points of the structure of *Toxodon*!" (Darwin 1845: 82)

The study of dental tissues is of great importance for understanding the life history and evolution of fossil mammals, being widely used in taxonomic, phylogenetic, palaeobiological, and palaeoecological studies. Dental enamel microstructure is important for the inference of phylogenetic relationships, to identify higher orders of mammalian taxa and to document intraindividual and intraspecific variability for comparative purposes (e.g., Kawai 1955; Koenigswald et al. 1987; Koenigswald and Sander 1997b; Ferretti 1999; Steffen 1999; Wood et al. 1999; Tabuce et al. 2007; Vieytes et al. 2007; Alloing-Séguier et al. 2014; Koenigswald and

Krause 2014; Bergqvist and Koenigswald 2017; Braunn and Ribeiro 2017 and references therein). Furthermore, dental histological analyses are also useful for determining the relationship between enamel microstructure and biomechanical stress patterns (e.g., Rensberger and Koenigswald 1980; Koenigswald et al. 1987; Pfretzschner 1988, 1992; Koenigswald 1992; Rensberger 1995; Steffen 1999).

The microstructural organization of mammalian enamel consists of elongated hexagonal prisms (rods) and a material that lies outside the prism boundaries, the interprismatic matrix (IPM; interrods). The prisms result from columnar discordances in the hydroxyapatite crystal directions of the enamel (Rensberger 2000), and the IPM is compositionally identical to prismatic enamel but does not form prisms (Maas and Thewissen 1995). Four hierarchical structural levels of enamel are observed in mammals: (i) crystallites; (ii) prisms; (iii) enamel types; and (iv) the organization of the different types of enamel, named Schmelzmuster, determined by the arrangement of the prism groups (Fortelius 1985; Koenigswald 1988; Koenigswald and Clemens 1992; Koenigswald and Sander 1997a; Maas 1997; Lindenau 2005).

The notoungulates form a monophyletic group of South American native ungulates whose oldest record is *Archaeogaia macachaae* Zimicz, Fernández, Bond, Chornogubsky, Arnal, Cárdenas, and Fernicola, 2020, from Salta Province, NW Argentina (early–middle Paleocene). The radiation of Notoungulata is well recorded from the early Eocene (Bauzá et al. 2019), during the Itaboraian South American land mammal age (SALMA; 55.8 Ma ago), to the late Pleistocene–early Holocene, with a decline in diversity during the Pliocene (e.g., Cifelli 1985, 1993; Bond 1986; Croft et al. 2020). Billet (2011) presented a phylogenetic analysis in which Notoungulata is a well-supported clade; the monophyly of the well-known suborders Typotheria and Toxodontia is also supported. Toxodontia is recorded from the Eocene to early to middle Holocene, with only four genera reaching the Pleistocene in South America: *Toxodon* Owen, 1837, *Piauhytherium* Guérin and Faure, 2013, *Trigodonops* Kraglievich, 1931, and *Mixotoxodon* Van Frank, 1957, the latter being also found in Central and North America during the Pleistocene (Lundelius et al. 2013). *Toxodon*, the type genus of the subfamily Toxodontinae, had its last representatives associated with human remains in late Pleistocene and Holocene deposits (Marshall et al. 1984; Tonni et al. 1992; Guidón et al. 1994; Politis and Gutiérrez 1998; Politis et al. 2016).

The euhypsodont *Toxodon* was an large-sized herbivore (~1790 kg; Elissamburu 2012) recorded in various South American countries, such as Argentina, Uruguay, Venezuela, Brazil (Bond et al. 1995; Bond 1999), Bolivia (Paula-Couto 1979) and Paraguay (Hoffstetter 1978; Carlini and Tonni 2000). *Toxodon* means "bow-tooth" (named for its bow-like curved upper and lower teeth), and it exhibits a strongly projected rostrum, with flattened upper and lower incisors (Owen 1837). The ever-growing teeth of *Toxodon* have open-roots, with continuous growth of enamel and dentine throughout the lifetime of these animals; enamel is arranged in longitudinal areas of variable length, interspersed with areas devoid of enamel, mainly on the lingual face of the teeth (Paula-Couto 1979; see fig. 1 in SOM 1, Supplementary Online Material available at http://app.pan.pl/SOM/app66-Braunn_etal_SOM.pdf).

Studies on the enamel microstructure of Toxodontia are still sparse, but they are essential to analyse biomechanical features, dietary habits, and phylogenetic and taxonomic relationships, as well as to reconstruct biological rhythms (e.g., Fortelius 1985; Pfretzschner 1994; Maas 1997; Lindenau 2005; Braunn et al. 2014; Madden 2015; Fillippo et. al 2020). In this study we analyse teeth of *Toxodon* collected in Pleistocene deposits of São Paulo State and the Coastal Plain of Rio Grande do Sul State, Brazil (Santa Vitória Formation; late Pleistocene), in order to address two main goals: (i) describe the dental enamel microstructure of *Toxodon* sp. in adult and juvenile specimens using scanning electron microscopy (SEM), and (ii) discuss the evolutionary and functional implications of histological enamel features in these euhypsodont teeth.

Institutional abbreviations.—MCN-PV (MCN-PHIS), Museu de Ciências Naturais, Secretaria do Meio Ambiente e Infraestrutura, Porto Alegre, Brazil; MCTFM-PV, Museu Coronel Tancredo Fernandes de Mello, Santa Vitória do Palmar, Brazil; MN-V, Museu Nacional, Universidade Federal do Rio de Janeiro, Rio de Janeiro, Brazil.

Other abbreviations.—I, i, upper and lower incisors; dP and dp, deciduous upper and lower premolars; p, lower premolar; M and m, upper and lower molars (the number following the tooth abbreviation indicates the position along the dental arcade). EDJ, enamel-dentine junction; HSB, Hunter-Schreger bands; IPM, interprismatic matrix; MRE, modified radial enamel; NNL, neonatal line; OES, outer enamel surface; RE, radial enamel.

Material and methods

Studied material.—In this study, 13 upper and lower teeth of *Toxodon* sp. were selected for SEM imaging from the

Fig. 1. Enamel microstructure in upper and lower incisors of *Toxodon* sp. from the upper Pleistocene of Rio Grande do Sul (southern Coastal Plain, Santa Vitória Formation) and São Paulo states, Brazil. Scanning electron micrographs of longitudinal (A, B) and transversal (C, D) sections through the uppermost and labial side of the dental axis. **A**. MCN-PV 1162.PHIS-54, I2, general view of the intermediary layer of enamel with Hunter-Schreger bands and modified radial enamel associated to the enamel-dentine junction. **B**. MCN-PV 9907.PHIS-53, I1, radial enamel with prisms parallel between them close to outer enamel surface (B_1), innermost zone of the enamel (B_2). **C**. MCN-PV 9879.PHIS-56, i3, Hunter-Schreger bands and modified radial enamel, with IPM surrounding the prisms. **D**. MN 2372-V.C.PHIS-003, i1, detail of modified radial enamel (D_1), oval aspect of prisms in cross-section (D_2). Dashed lines indicate the morphology of enamel-dentine junction. →

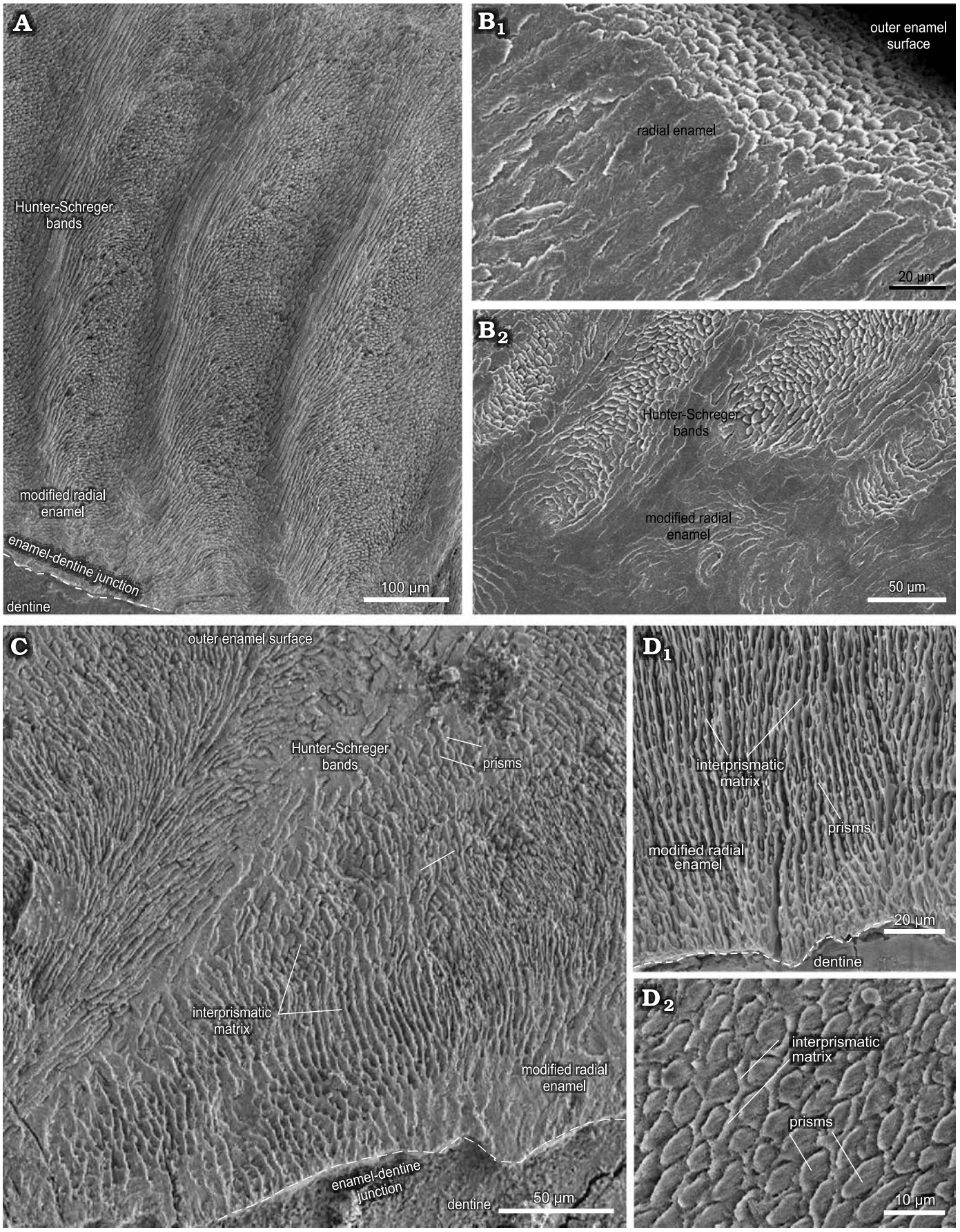
A
Hunter-Schreger bands
modified radial enamel
enamel-dentine junction
dentine
100 µm
B1
outer enamel surface
radial enamel
20 µm
B2
Hunter-Schreger bands
modified radial enamel
50 µm
C
outer enamel surface
Hunter-Schreger bands
prisms
interprismatic matrix
modified radial enamel
enamel-dentine junction
dentine
50 µm
D1
interprismatic matrix
prisms
modified radial enamel
20 µm
dentine
D2
interprismatic matrix
prisms
10 µm

palaeontological collections of the Museu de Ciências Naturais of the Secretaria do Meio Ambiente e Infraestrutura (Porto Alegre), Museu Coronel Tancredo Fernandes de Mello (Santa Vitória do Palmar), and Museu Nacional of the Universidade Federal do Rio de Janeiro (Rio de Janeiro). The specimens include incisors, premolars, and molars from late Pleistocene deposits of Rio Grande do Sul (Santa Vitória Formation) and São Paulo states. The histological dental material examined includes 56 histological sections of maxillary and mandibular teeth (I1, I2, M3, i1, i3, p4, m1–2, dP4 and dp4). Parallel sections along the longitudinal tooth axis, transversal sections and more than one tangential section were taken when possible (see Table 1; SOM 2).

Dental nomenclature.—Tooth terminology follows Madden (1997) (fig. 1 in SOM 1). Enamel microstructural terminology follows Koenigswald and Sander (1997a).

Preparation of specimens.—Teeth were embedded in polyester resin, and the blocks were cut transversely and longitudinally with a diamond saw (Buehler Petro-Thin, Thin Sectioning System) at the Laboratory of Mineralogy of the Universidade Federal de Pelotas (Pelotas, Rio Grande do Sul, Brazil). Sections were polished with 600–2500 grit carborundum powder. Prior to SEM imaging, the specimens were etched with 1N HCl for 120 seconds, and subsequently washed in distilled, deionized, and fresh water for 5 minutes. A second acid treatment was performed, using 34% v/v phosphoric acid for 3 seconds. Preparation of the specimens was performed in the Palaeontology Section of the Museu de Ciências Naturais, Secretaria do Meio Ambiente e Infraestrutura (Porto Alegre, Rio Grande do Sul, Brazil). After the sections dried, they were mounted on aluminium stubs, sputter-coated with gold and viewed in a JEOL JSM 6060 SEM operated at an accelerating voltage of 10 kV. The SEM imaging of the samples was performed using secondary electron imaging modes. Measurements were taken from SEM micrographs using the Image J software. All teeth are oriented with the occlusal surface directed upwards in the scanning micrographs. Microscopic analyses were performed at the Centro de Microscopia e Microanálise of the Universidade Federal do Rio Grande do Sul (Porto Alegre, Rio Grande do Sul, Brazil). Histological sections obtained from this study were deposited in Museu de Ciências Naturais (Porto Alegre) palaeontological collection under the MCN-PHIS acronym. palaeontological collection under the MCN-PHIS acronym.

Results

Enamel from the permanent teeth I1, I2, M3, i1, i3, p4, and m1–2 (Figs. 1–3) and deciduous teeth dP4 and dp4 of *Toxodon* sp. (Fig. 4) exhibit Schmelzmuster with three enamel types, in which the orientation of the prisms, relative thickness and IPM vary: an innermost layer associated with the EDJ, corresponding to MRE; an intermediary layer formed by decussating prisms, consisting of regularly distributed HSB; and a layer of RE next to the OES. Detail of enamel microstructure features can be observed in scanning micrographs presented in SOM 3: figs. 1–11.

Upper incisors.—The enamel microstructural data for the upper incisors were obtained from longitudinal sections of two specimens, I1 (MCN-PV 9907) and I2 (MCN-PV 1162), from which two histological sections were studied (Fig. 1A, B; see also SOM 2: table 1).

In I1, the total enamel thickness varies from ~970–1000 μm, and three enamel types are observed: MRE (18%), HSB (60%) and RE (22%) (Figs. 1B, 5A). The MRE is characterized by decussation of the IPM and prisms, forming thick plates among them, and it is not possible to distinguish one from the other (Fig. $1B_2$). Prisms in the HSB extend outward from the MRE with an inclination of ~60–70° in relation to the EDJ, and the number of prisms varies from about 6–9 per band (Fig. $1B_2$). The RE exhibits prisms oriented at the same angle as the OES and rises apically from the HSB (Fig. $1B_1$). The EDJ is smooth, without ridges, apparently devoid of scallops, but with tiny spikes and depressions in the dentinal areas under the enamel.

In I2 (Fig. 1A), the total enamel thickness in the apical portion of the dental axis varies from about 1170–1320 μm, while in the labial side the thickness makes 1050–1070 μm. It is not possible to analyse the data regarding the total thickness of each enamel type from the apical portion of the I2 in the photomicrographs obtained. In the labial side of the dental axis, three enamel types are observed: MRE (10%), HSB (53%), and RE (37%) (Figs. 1A, 5B). The MRE exhibits thick plates of IPM between the prisms, which are oriented parallel to each other. The prisms in the HSB tend to be straight and directed cervically, at an angle of about 45–65° in relation to the EDJ; the number of prisms varies from about 9–14 per band, alternating with a layer of prisms distributed perpendicularly (Fig. 1A). In the intermediary layer of enamel located near the apical portion of the dental axis, the prisms exhibit an undulating pattern. Prisms of RE are distributed parallel to each other and apically to the external surface of the dental axis. The EDJ presents small undulations in the labial side of the incisor (Fig. 1A) and develops scallops in the apical area.

Lower incisors.—Transversal and longitudinal sections of lower incisors were obtained from three specimens, i1 (MN 2372-V.C), i3 (MCN-PV 9879), and i? (MN 2938-V), from which 11 histological sections were studied (Fig. 1C, D; SOM 2: table 1).

In i1 (Fig. $1D_1$), the total enamel thickness varies from about 1120–1420 μm in the mesial portion of the dental axis, and from about 670–1000 μm in the distalmost area of the buccal face. In the longitudinal sections through the mesial surface of the dental axis, three enamel types are observed: MRE (15%), HSB (55%), and RE (30%) (Fig. 5C). The HSB are at an angle of 70° in relation to the EDJ, and there are about 15–20 prisms per band. In the transversal sections

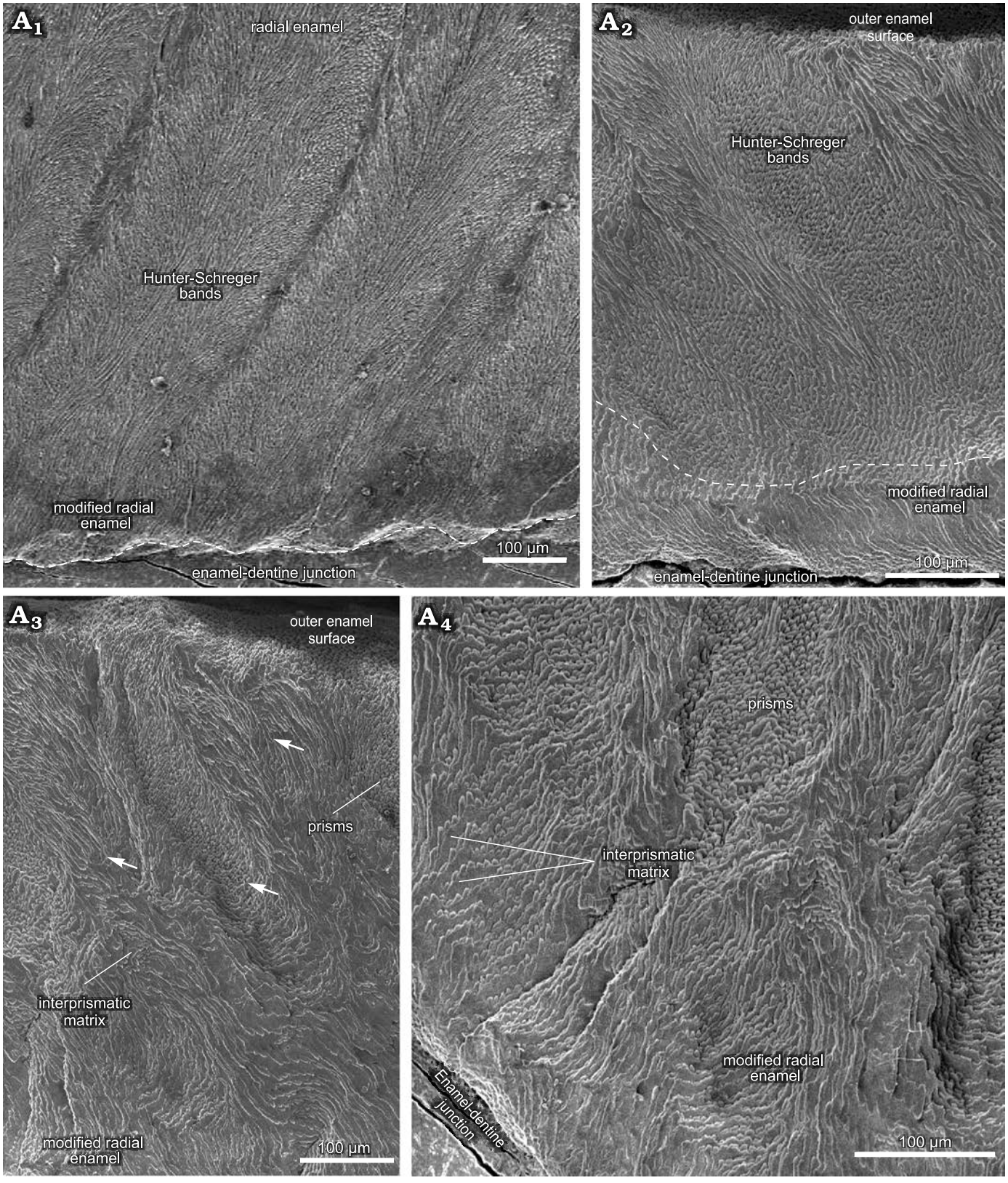

Fig. 2. Enamel microstructure in upper molar of *Toxodon* sp. from the upper Pleistocene of Rio Grande do Sul State, Brazil (southern Coastal Plain, Santa Vitória Formation). Scanning electron micrographs of transversal sections of the ectoloph (A_1) and paracone, including the anterior fold (A_2–A_4). MCN-PV 30077.PHIS-055, M3, general view of enamel exhibiting Schmelzmuster with three enamel types (A_1), Hunter-Schreger bands in the enamel of loop from anterior fold on the protocone and modified radial enamel below the dashed line (A_2), enamel of outermost loop from anterior fold on the metacone, in opposite position to that observed in A_2 (A_3, A_4). Arrows indicate difference in depth between Hunter-Schreger bands. Dashed line in A_1 indicates the morphology of enamel-dentine junction.

through the distal portion of the first lower incisor, it is possible to observe that the relative thickness of the three types of enamel varies: MRE constitutes 32% where the enamel is thinner and about 16–22% in regions where it is thicker; HSB exhibit a greater thickness, 58–66%, where the enamel is thicker and about 36% in areas where it is thinner; and RE constitutes 28–32% where the enamel is thinner and 18–30% in thicker areas (Fig. 5D). MRE with thick plates of IPM between the prisms is visible in the longitudinal sections through the distal portion, while in the transversal sections, vertical rows of prisms could be observed oriented perpendicular to the thick IPM plates that surround all sides with an equal thickness. In longitudinal sections through the lowermost mesial portion of the dental axis, the HSB are disposed as an intermediary layer of enamel and show an undulating pattern due to the transitional zones between individual bands, separated from each other by bifurcations. In a higher magnification image of this area of enamel, it is possible to observe that the transitional bands exhibit thin plates of IPM perpendicular to the prisms. HSB show an undulating pattern in a tangential section. In longitudinal sections through the distal portion of the dental axis, the prisms in the HSB tend to be straight and directed cervically, at an angle of about 45–60° in relation to the EDJ, and the number of prisms varies from 8–10 per band. The RE exhibits enamel incremental lines in longitudinal sections. RE occupies about 26–32% of the total thickness of enamel in the thicker areas and 18% in the thinner areas. Prisms of the RE close to the OES exhibit an angle of 45° in relation to the EDJ. The EDJ has a smooth appearance devoid of scallops (Fig. $1D_1$).

In i3 (Fig. 1C, D_2), the total enamel thickness varies from about 720–890 μm, and transversal sections of the uppermost portion through the dental axis exhibits three enamel types: MRE (12%), HSB (56%), and RE (32%) (Fig. 5E). The MRE exhibits prisms formed by wide plates of IPM between radial rows of prisms, being difficult to differentiate between them in some areas (Fig. 1C). There are 10 prisms per band in each HSB, and the prisms tend to be straight and directed cervically from the MRE to RE, at an angle of about 45–55°. HSB extend from the MRE and reach the OES in some areas. It is possible to observe in the RE that in transversal cross-sections the enamel prisms appear to have an oval aspect; open prism sheaths are composed of IPM that surrounds them (Fig. $1D_2$). Tangential sections show prisms of RE distributed parallel to each other and close to the OES. The EDJ in this lower incisor displays small scallops (Fig. 1C) or undulations.

Upper molar.—The microscopic analysis of the upper molar was performed through transversal sections of an M3 (MCN-PV 30077), from which two histological sections were obtained (Fig. 2; see also SOM 2: table 1).

Transversal sections through the upper portion of the ectoloph and paracone, including the anterior fold, next to the occlusal surface, showed that the Schmelzmuster differs on the buccal and lingual sides of the M3 (Fig. 2). On the buccal side of the dental axis, the thickness of the enamel on the ectoloph is about 1000 μm, and three enamel layers are observed: MRE (24%), HSB (56%), and RE (20%) (Figs. $2A_1$, 6A). The MRE exhibits large plates of IPM, and it is not possible to distinguish prisms. The angle of inclination of the HSB varies from about 45–50°, with 7–12 prisms per band (Fig. $2A_1$). The RE in the buccal enamel of the ectoloph is composed of crystallites of IPM parallel to the prism direction at an angle of 90° in relation to the EDJ.

The thickness of the lingual enamel on the anterior fold of the M3 varies from about 390 to 810 μm, where only two layers are observed: MRE (20%) and HSB (80%) (Figs. $2A_2$–A_4, 6B). The MRE is characterized by thick plates of IPM perpendicular to the prisms (Fig. $2A_2$–A_4). The HSB are distributed from the MRE to the OES with an inclination angle of 45° in relation to the EDJ, and has about 6 to 13 prisms per band (Fig. $2A_2$). In the enamel on the distal loop of the anterior fold of the metaloph, the HSB are composed of bands with decussating prisms that are thicker than those formed by vertical prisms (Fig. $2A_2$), while on the mesial loop of the protocone, bands formed by vertical prisms are thicker than those composed of decussating prisms, with a difference in depth between them (Fig. $2A_3$, A_4). Regarding the shape of the EDJ, it is possible to observe a scalloped outline of enamel on the dentine (Fig. $2A_1$, A_2).

Lower premolars and molars.—The microscopic analysis of the lower cheek teeth was conducted through transversal and tangential sections on the buccal side of the p4 and m1–2, from which three histological sections were obtained (Fig. 3; see also SOM 2: table 1). The first and second lower molars were treated as belonging to a same dental category (m1–2) due to their morphological resemblance.

In p4, the total thickness of the buccal enamel is about 1200–1280 μm, while the enamel on the buccal enamel fold varies 430–960 μm. The enamel types include MRE (7%), HSB (53%), and RE (40%) (Fig. 6C). In the MRE, large plates of IPM perpendicular to the prisms are observed. The HSB have a regular distribution, at an angle of about 40–50°, and with 15–20 prisms per band. Prisms in the RE are parallel to each other close to the external surface. The EDJ exhibits moderate undulations.

Fig. 3. Enamel microstructure in m1–2 of *Toxodon* sp. from the upper Pleistocene of Rio Grande do Sul State, Brazil (southern Coastal Plain, Santa Vitória Formation). Scanning electron micrographs of transversal (A) and tangential (B_1–B_6) sections of the buccal and lingual sides through of the dental axis, respectively. **A**. MCN-PV 9902.PHIS-059, general view of the enamel and dentine of the hypoconulid showing Schmelzmuster with three enamel types. **B**. MCN-PV 9902.PHIS-052, enamel and dentine of innermost loop from the meta-entoconid fold (B_1). Note the Hunter-Schreger bands along the enamel fold (B_1, B_2), enamel and dentine from the ento-hypoconulid fold exhibiting hypoplastic defects (asterisks) (B_3, B_4), higher magnifications of deep hypoplastic defect observed in B_3 (inside the box; distal loop of fold) (B_4), enamel in the mesial loop of the fold exhibiting Schmelzmuster with three enamel types (B_5); detail of modified radial enamel with enlarged empty spaces (white arrows and asterisks) (B_6). Dashed lines indicate the morphology of enamel-dentine junction. →

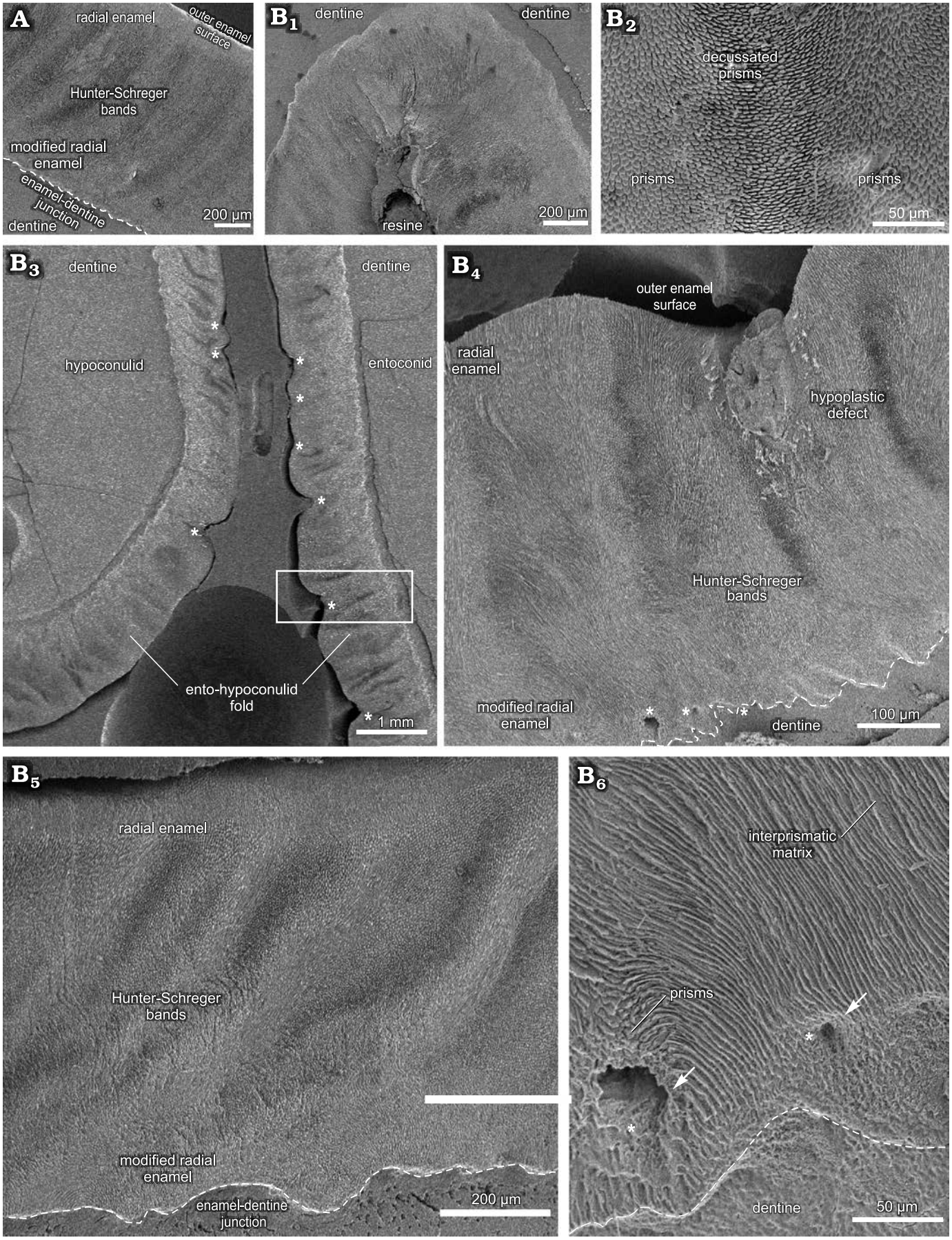
A
radial enamel
outer enamel surface
Hunter-Schreger bands
modified radial enamel
enamel-dentine junction
dentine
200 µm
B1
dentine
dentine
resine
200 µm
B2
decussated prisms
prisms
prisms
50 µm
B3
dentine
dentine
hypoconulid
entoconid
ento-hypoconulid fold
1 mm
B4
outer enamel surface
radial enamel
hypoplastic defect
Hunter-Schreger bands
modified radial enamel
dentine
100 µm
B5
radial enamel
Hunter-Schreger bands
modified radial enamel
enamel-dentine junction
200 µm
B6
interprismatic matrix
prisms
dentine
50 µm

In mesial molars (m1–2), the results were obtained from transversal and tangential sections through the uppermost portion of the dental axis, from which measurements of the buccal, mesial and lingual enamel were taken for comparative analysis, including the lingual enamel folds (Fig. 3). On the hypoconulid, in the distalmost portion of the buccal side of the mesial molars, the enamel thickness varies from about 1150–1380 μm, with three enamel types: MRE (10%), HSB (60%), and RE (30%) (Figs. 3A, 6D). The enamel thickness along the buccal enamel in the talonid varies from about 640–1760 μm, the thinner areas being close to the buccal enamel fold. The MRE is composed of vertical rows of prisms oriented parallel to the IPM that surrounds all sides with an equal thickness. The HSB exhibit thicker and thinner alternate vertical bands at an angle of 60–65° in relation to the EDJ, with 5–6 prisms per band. Bands formed by vertical prisms are thicker than those composed of decussating prisms (Fig. 3A). RE close to the OES is composed of prisms parallel to each other (Fig. 3A). The EDJ in this portion of the dental axis of the lower molar exhibits a more scalloped configuration than in the lower premolars (Fig. 3A).

Through microscopic analysis of a tangential section through the meta-entoconid fold of the m1–2, it is possible to observe variation in the enamel thickness (Figs. 3B$_1$, 6E, F, I–K). The mesial and distal loops of the meta-entoconid fold present thinner areas close to the internal portion of the fold: in the mesial loop (innermost area), the enamel thickness varies from about 540–680 μm, and only two enamel layers are observed: MRE (44%) and HSB (56%) (Fig. 6E), while in the internal portion of the fold the thickness is about 500–900 μm, with three types of enamel: MRE (22%), HSB (63%), and RE (15%) (Fig. 6F). In the mesial loop of this enamel fold, the thickness is about 600–740 μm, with MRE (33%), HSB (45%), and RE (22%) (Fig. 6K). On the distal loop, the thickness is 890–1230 μm, with MRE (43%), HSB (38%), and RE (19%) (Fig. 6I), while in the innermost area of the distal loop, the thickness is about 780–820 μm, with MRE (14%), HSB (49%) and RE (37%) (Fig. 6J). The MRE is composed of thin plates of IPM between rows of perpendicular prisms. The HSB in the internal portion of the fold exhibit an undulating pattern parallel to the EDJ (Fig. 3B$_1$, B$_2$), with alternate rows of about 6–20 prisms in decussating areas and thin layers of IPM between them; prisms are at an angle of about 45° to the IPM that surrounds all sides with an equal thickness (Fig. 3B$_2$). The angle of inclination of the HSB varies between the mesial and distal loops of the meta-entoconid fold: in the mesial loop it is about 25–50°, while in the distal loop it is about 75–90°, reaching 60–70° in areas close to the internal portion of the fold, with 10 to 20 prisms in each band. The RE is formed by prisms parallel to each other at an angle of about 45 to 90° in relation to the EDJ. The outline of the EDJ presents a pronounced scalloped outline along the meta-entoconid fold (Fig. 3B$_1$).

In a tangential section through the ento-hypoconulid fold of the m1–2, the total enamel thickness varies from 210–1120 μm; the thicker areas are in the internal (840–1120 μm) and distal (830–950 μm) loops of the fold, while in the mesial loop the thickness is about 210–830 μm (Fig. 3B$_3$; SOM 2: table 1). It is not possible to observe Schmelzmuster in the internal loop of the ento-hypoconulid fold, while in the mesial loop there are three enamel types: MRE (32%), HSB (51%), and RE (17%) (Fig. 6H); the distalmost loop of the ento-hypoconulid fold shows different thicknesses of the enamel layers: MRE (23%), HSB (50%), and RE (27%) (Fig. 6G). Along the external surface of the ento-hypoconulid fold there are various hypoplastic defects (Fig. 3B$_3$, B$_4$). In the MRE, characterized by large plates of IPM covering the prisms, enlarged empty spaces are also observed, indicative of defects in the mineralization of the enamel prisms (Fig. 3B$_3$, B$_4$). HSB in the mesial loop of the ento-hypoconulid fold are distributed at an angle of 45–50° in relation to the EDJ, with 14–18 prisms in each band (Fig. 3B$_3$, B$_5$), while in the distal loop, the bands exhibit angles of 60–65° and 4–12 prisms (Fig. 3B$_3$, B$_4$). Prisms in the RE are parallel to each other close to the external surface of the enamel fold. In both loops of the ento-hypoconulid fold, the EDJ shows a pronounced scalloped outline (Fig. 3B$_4$–B$_6$).

Deciduous teeth.—The enamel microstructural analysis of the upper and lower deciduous premolars was performed through transversal and longitudinal sections of three dP4 (MCN-PV 36937, MN 2372-V.A, and MN 2372-V.B) and one dp4 (MCTFM-PV 793), from which nine histological sections were studied (Fig. 4; see also SOM 2: table 1).

Upper deciduous premolars: In dP4, the results were obtained from transversal and longitudinal sections through the lowermost portion of the dental axis. Measurements were taken from the buccal and lingual enamel for comparative analysis, including the lingual enamel folds (Figs. 4, 7A–D; SOM 2: table 1).

In specimen MCN-PV 36937, for both the transversal and longitudinal sections through the buccal enamel on the ectoloph, the enamel thickness varies from 480–650 μm. Longitudinal sections through the distalmost portion of the ectoloph show three enamel types: MRE (33%), HSB (48%) and RE (19%) (Fig. 7A). The MRE is formed by thick plates of IPM between the prisms at an angle of 45° (Fig. 4A$_1$). HSB are at an angle of 45–55° in relation to the EDJ and are formed by bands of intersected prisms with different thicknesses (about 9–12 prisms in each band) alternating with

Fig. 4. Enamel microstructure in upper and lower deciduous premolars of *Toxodon* sp. from the upper Pleistocene of Rio Grande do Sul (southern Coastal Plain, Santa Vitória Formation) and São Paulo states, Brazil. Scanning electron micrographs of longitudinal (A$_1$, A$_2$, B, C$_1$) and transversal (A$_3$, C$_2$) sections of the dental axis. **A**. MCN-PV 36937, dP4 (A$_1$, A$_2$, PHIS-44): general view of buccal enamel and dentine from the ectoloph exhibiting three enamel layers (A$_1$), distal loop of anterior fold, exhibiting weakly developed Hunter-Schreger bands (A$_2$), mesial loop of anterior fold on the protocone with thick plates of interprismatic (white arrows) from the enamel-dentine junction up to the outer enamel surface (A$_3$, PHIS-46). **B**. MN 2372-V.B.PHIS-24, dP4: lingual enamel on the protoloph exhibiting Schmelzmuster with two enamel types. Neonatal line with orifices of dentinal tubules under the beginning →

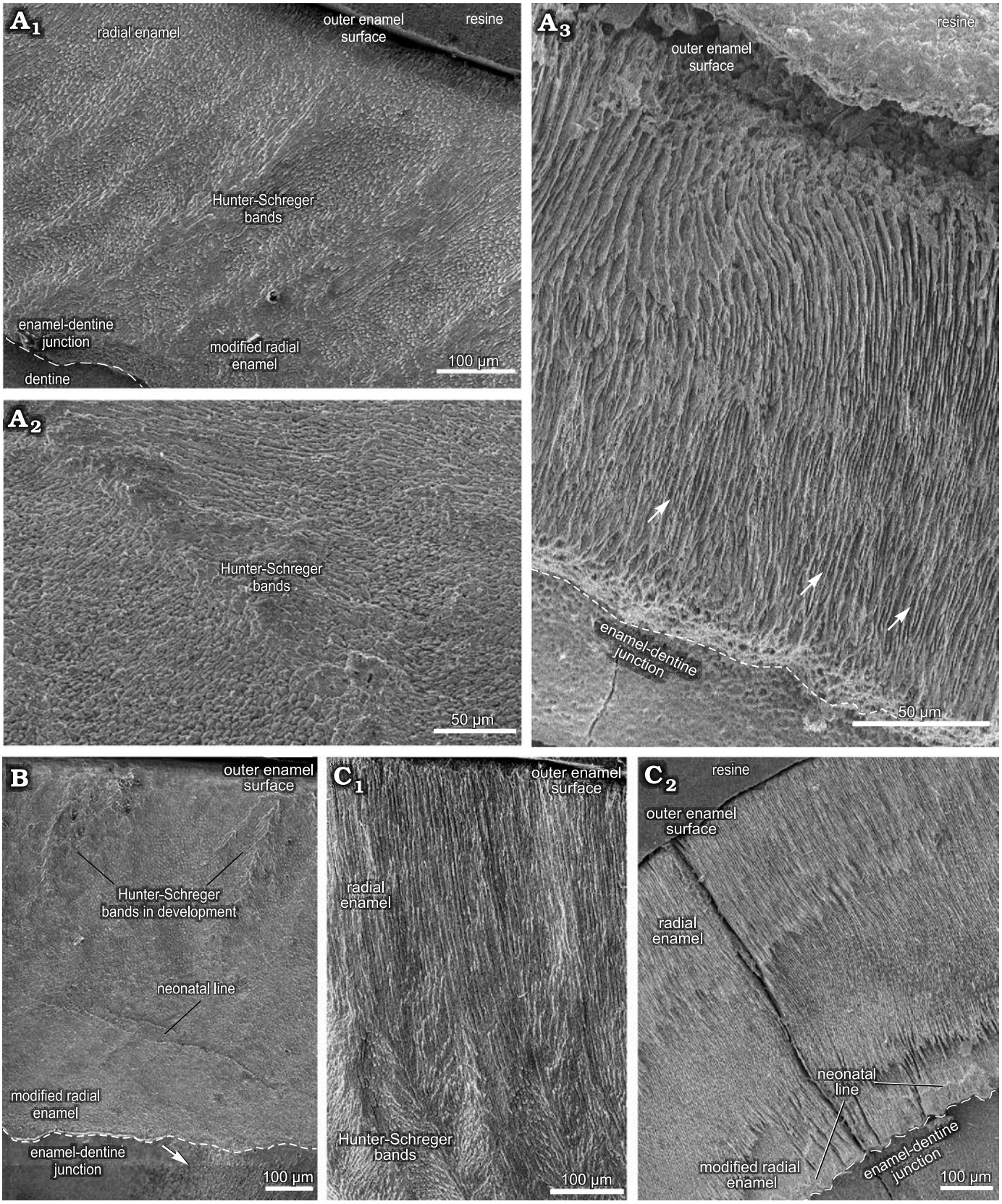

of a defect (white arrow). **C**. MCTFM-PV 0793, dp4: partial view of buccal enamel on the paraconid (C_1, PHIS-30), overview of lingual enamel on the para-metaconid fold showing radial distribution of prisms from the enamel-dentine junction to the outer enamel surface. Neonatal line parallel and close to the enamel-dentine junction (white arrows). Note the enamel fissure between the enamel prisms and dentine (C_2, PHIS-50). Dashed lines indicate the morphology of enamel-dentine junction.

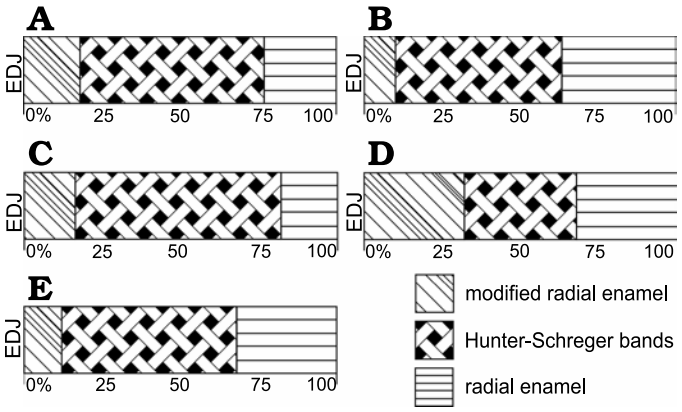

Fig. 5. Diagrammatic representation indicating microstructural variation of buccal enamel in upper (A, B) and lower (C–E) incisors of *Toxodon* sp. **A**. I1. **B**. I2. **C**, **D**. i1. **E**. i3. Areas close to mesial (C) and distal (D) portions of the dental axis. Illustration based on Lindenau (2005). Abbreviation: EDJ, enamel-dentine junction.

thin layers of IPM (Fig. $4A_1$). The RE exhibits prisms that are parallel to each other (Fig. $4A_1$). The EDJ shows a pronounced scalloped outline (Fig. $4A_1$). The enamel thickness of the buccal enamel on the ectoloph is about 520–650 μm; however, the microstructural features of this area of enamel could not be observed in the transversal sections obtained.

The thickness observed in a longitudinal section of the lingual enamel on the distal loop of the anterior fold is about 680–840 μm. It is possible to observe weakly developed HSB, formed by apposition of the IPM layers (Fig. $4A_2$). In a transversal section through the lingual enamel on the distal loop of the anterior fold, the thickness varies 330–440 μm, exhibiting only RE (Fig. $4A_3$). Enamel thickness varies 210–720 μm in the mesial loop of the anterior fold on the protocone, and from the EDJ to the OES it is not possible to view the prisms, except for an area close to the EDJ, where some prisms are parallel to the thick plates of IPM (Fig. $4A_3$). The distal loop of the anterior fold on the metaloph of the dP4 exhibits thick plates of IPM from the EDJ to the OES, and it is not possible to differentiate prisms between them. The EDJ is scalloped in both the buccal enamel on the ectoloph and the lingual enamel of the anterior fold on the protocone (Fig. $4A_1$). The enamel thickness decreases in the distalmost lingual folds: both loops of the posterior fold have thicker enamel (220–440 μm), while the distalmost enamel on the metaloph is thinner (210–280 μm), but enamel features could not be observed.

In the specimens of dP4 from the State of São Paulo, MN 2372-V.A and MN 2372-V. (Fig. 4B), the thickness of the lingual enamel on the protoloph is about 610–840 μm, and the enamel exhibits Schmelzmuster with two layers: MRE (17%) and HSB (83%) (Figs. 4B, 7B). The MRE has

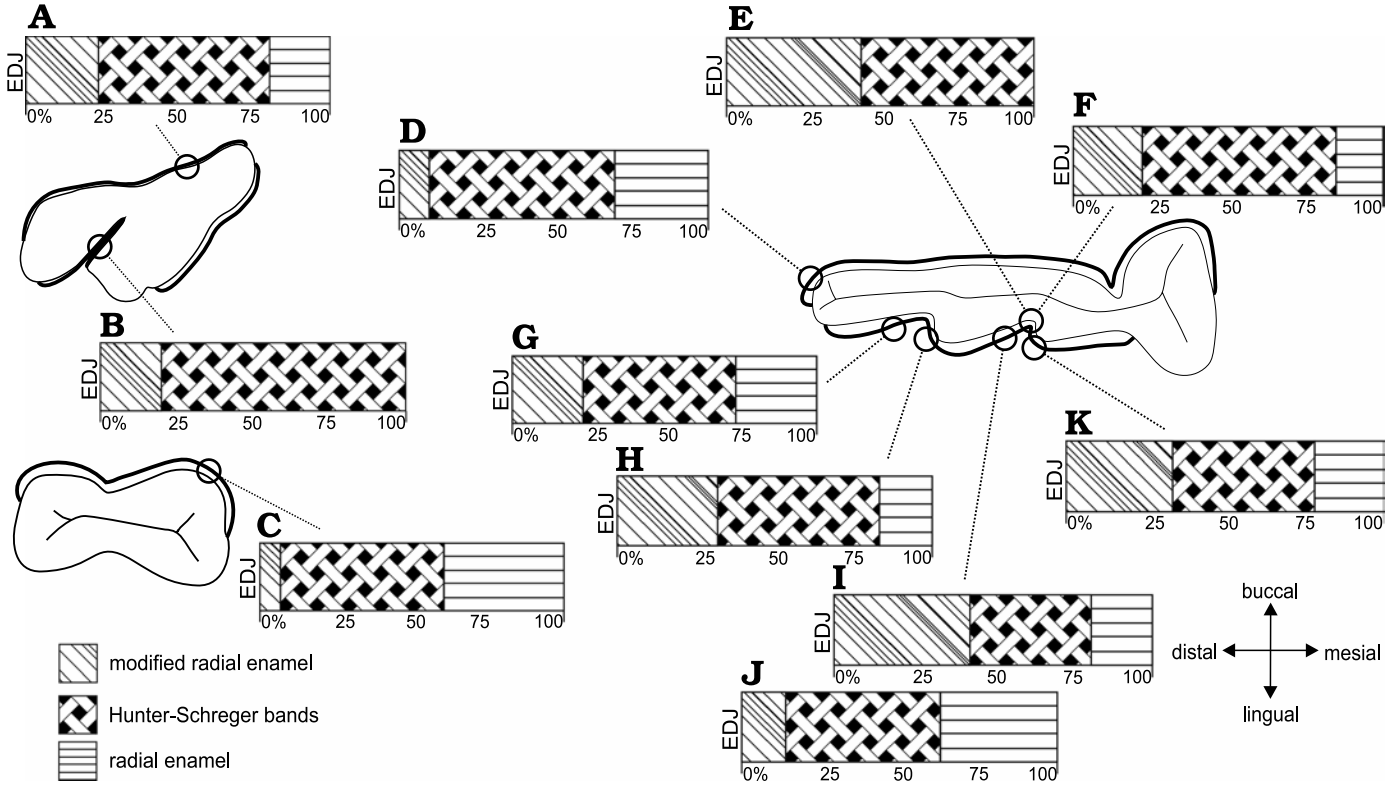

Fig. 6. Diagrammatic representation indicating microstructural variation of enamel in upper permanent molar (A, B) and lower permanent premolar (C) and molar (D–K) of *Toxodon* sp. **A**, **B**. M3. **C**. p4. **D**–**K**. m1–2. Symbols represent different percentages of enamel zones from the enamel-dentine junction (EDJ) up to the outer enamel surface. **A**. Ectoloph (mesial distal). **B**. Anterior fold (distal). **C**. Buccal enamel. **D**. Hypoconulid. **E**. Meta-entoconid fold (mesial loop close to internal portion of fold). **F**. Meta-entoconid fold (distal loop close to internal portion of fold). **G**. Ento-hypoconulid fold (mesial loop). Illustration based on Lindenau (2005). **H**. Ento-hypoconulid fold (distal loop). **I**. Meta-entoconid fold (distal loop). **J**. Meta-entoconid fold (innermost area of the distal loop). **K**. Meta-entoconid fold (internal portion).

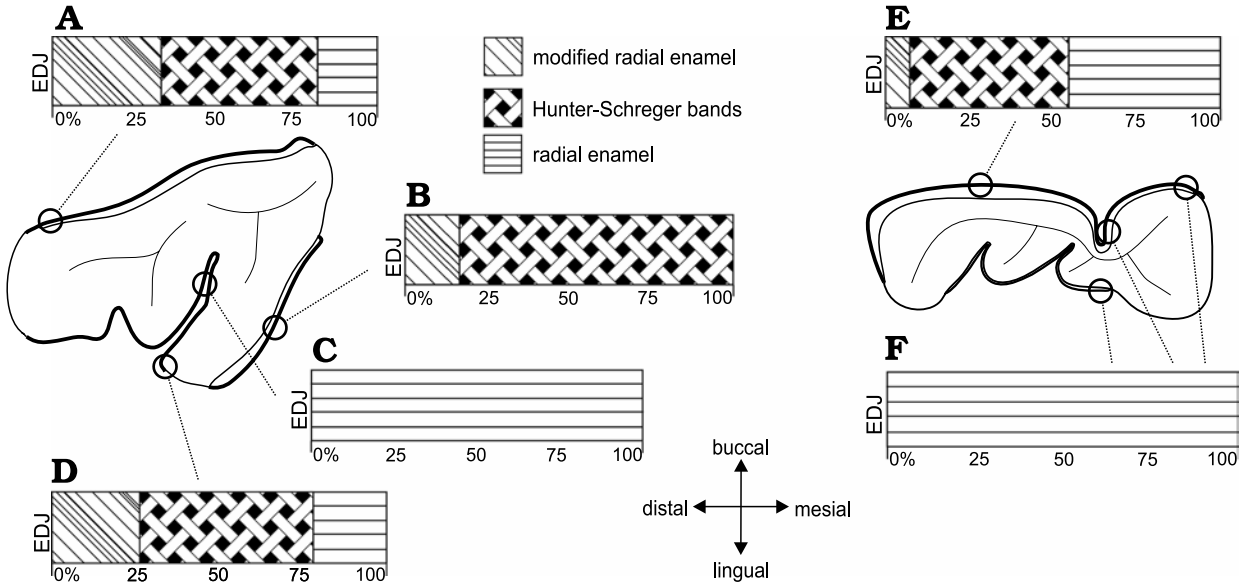

Fig. 7. Diagrammatic representation indicating microstructural variation of buccal and lingual enamel from distinct regions of the dental axis in upper (dP4, **A**–**D**) and lower (dp4, **E**, **F**) deciduous premolars of *Toxodon* sp. Symbols represent different percentages of enamel zones from the enamel-dentine junction (EDJ) up to theouter enamel surface. Microstructural features are obtained from longitudinal (A, B) and transversal sections (C–E). Illustration based on Lindenau (2005).

rows of prisms at an angle of 45° in relation to the thick plates of IPM between them. A neonatal line extends from the MRE close to the EDJ up to the level of the intermediary layer of enamel with a "staircase" distribution pattern, where it is possible to identify the prisms formed prenatally and postnatally (below and above the defect, respectively). The prenatal enamel is not fully mineralized, with more irregular prisms exhibiting smaller diameters, and the postnatal prisms have a more regular pattern (Fig. 4B). HSB are regularly distributed at an angle of 45–55° in relation to the EDJ, and the bands of intersected prisms (composed of about 6–10 prisms) are weakly developed, indicating the early stages of enamel development (Fig. 4B). In the lingual enamel of the innermost loop of the anterior fold, and above this area, the enamel prisms are parallel to the IPM, without an intersection between them (Fig. 7C). In the lingual enamel on the protocone there are three types of enamel for a total thickness of 30–77 μm: MRE (26%), HSB (53%), and RE (21%) (Fig. 7D). It is not possible to distinguish prisms between the thick plates of IPM in the MRE. The EDJ on the protoloph and anterior fold is scalloped, while on the protocone the outline of the enamel under the dentine is straight.

Lower deciduous premolar: Enamel microscopic analyses of dp4 were made using transversal and longitudinal sections through the uppermost portion of the dental axis. Measurements were taken from the buccal and lingual sides of the dental axis, including the lingual enamel folds (Fig. 4C; see also SOM 2: table 1).

The thickness of the buccal enamel on the protoconid is about 760–990 μm, and although there are three enamel types in this area, it was not possible to determine the percentage of each in the photomicrographs obtained (Fig. 4C). In the same longitudinal section, the enamel thickness of the opposite lingual band on the paraconid is about 960–1410 μm, composed of prisms radially distributed from the EDJ to the external surface. The MRE has wide plates of IPM, but it is not possible to detect the prisms between them (Fig. $4C_1$). The HSB are distributed at an angle of about 45–60° and are composed of alternating thinner and thicker bands of vertical and decussating prisms (Fig. $4C_1$). Decussating bands have radial rows of about 5–10 prisms at an angle of 45° in relation to the plates of IPM (Fig. $4C_1$). RE is distributed in a wide portion of the enamel (Fig. $4C_1$). Buccal enamel thickness in the talonid is about 790–960 μm and in the trigonid 480–920 μm; the lower measurements were close to the buccal enamel fold, which is about 300 μm thick. The buccal enamel fold exhibits rows of prisms parallel to the IPM from the EDJ to the OES. A scalloped EDJ is observed.

The lingual enamel is thinner compared to that observed on the buccal side, where the lower measurements are from the meta-entoconid fold (290–450 μm) and from the mesial band of enamel on the protoconid (280–500 μm). The lingual enamel on the para-metaconid fold shows a radial distribution of prisms parallel to the IPM from the EDJ to the OES (Figs. 4C, 7F). It is possible to observe three distinct areas formed by narrow areas without prisms juxtaposed at different depths and a neonatal line, with a "staircase" distribution pattern, parallel to the scalloped EDJ (Fig. $4C_2$).

Discussion

Toxodontids are easily recognized by the arrangement of their anterior dentition, with large I1 and i1 protruding like a "shovel," and with I2 and i3 modified into tusks with

continuous growth (Madden 1997). Similar Schmelzmuster were observed in this study (among them the angle of inclination, number of prisms per band in the HSB and percentage occupied by enamel layers) for I1 and i1 (Fig. 5A, C), as well as I2 and i3 (Fig. 5B, E), suggesting similar points of contact that concentrated stress during the power stroke in these antagonistic teeth. On the other hand, differences in the Schmelzmuster were observed between the distalmost portion of the i1 and its antagonistic first upper incisor (Fig. 5A, D), possibly reflecting changes in tensile stresses in the uppermost and lateral areas of the dental axis in these animals.

Dental antagonistic contact areas in *Toxodon* are also inferred from the microstructural similarities in Schmelzmuster of the lingual enamel folds of the upper and lower molars, where the distal loop of the anterior fold (Fig. 6B) occludes with the mesial loop of the meta-entoconid fold (Fig. 6E). These findings agree with those proposed by Fortelius (1985) regarding the occlusal relationships in the cheek teeth of ungulates, where the posterior half of a lower tooth occludes with the midpart of its upper homologue, while the anterior half of a lower tooth occludes with the anterior quarter of its upper homologue and the posterior quarter of the preceding tooth.

In *Toxodon*, the orientation of the thick layers of radial rows of prisms, separated by ascending IPM in which the crystals are perpendicular to the prisms in the MRE, seems to counter the masticatory impacts that are concentrated on the adjacent enamel close to the EDJ, as proposed by Pfretzschner (1992) for large-sized hypsodont mammals. In Notoungulata, this type of enamel occurs in Toxodontia (Toxodontidae) and Typotheria (Archaeohyracidae, Hegetotheriidae, Interatheriidae, and Mesotheriidae), as reported by Lindenau (2005).

Hunter-Schreger bands, the most frequent form of prism decussation among placental mammals, are an optical phenomenon caused by properties of the crystallites within the prisms (Kawai 1955; Koenigswald et al. 1987, 2011) and constitute an important biomechanical property of the enamel for preventing fracture even with very heavy loads, as observed by Maas (1994), Maas and Thewissen (1995), Koenigswald (1997), Shimizu et al. (2005), and Ungar (2015). The vertical HSB orientation observed in the dentition of *Toxodon* has previously been reported in teeth of large herbivorous mammals with high occlusal stress (Boyde and Fortelius 1986; Pfretzschner 1988; Koenigswald et al. 1987, 2011; Rensberger 1995, 1997; Steffen 2001; Lindenau 2005; Line and Bergqvist 2005; Lucas et al. 2008; Chai et al. 2009), where it gives to the enamel more strength against impacts (Koenigswald 1992) and has an important role in resisting crack propagation (Koenigswald and Sander 1997b; Popowics et al. 2001). The findings of this study corroborate the fact that in most mammals with this type of decussation of enamel, the thickness is about 6 to 20 prisms per band, with larger mammals tending to have thicker HSB, as observed by Kawai (1955).

As proposed by Lynch et al. (2010) for human enamel, HSB packing densities (number of HSB per mm of amelodentinal junction length) are most concentrated in regions exposed to the greatest functional demand, such as the occlusal surfaces of posterior teeth used for chewing and the surfaces of maxillary and mandibular canines used for guiding mandibular movement. A similar condition is observed in the upper incisors (Fig. 1A), as well as in the lower premolar of *Toxodon*, which can be related to an increase in load during mastication in these teeth.

The patterns of decussation of the HSB observed in this study show regional variations in their distribution throughout the enamel, which are possibly related to biomechanical demands. Although Koenigswald and Sander (1997b) stated that in large mammals the Schmelzmuster normally does not differentiate between the leading and trailing edges, in the upper molars of *Toxodon*, there are differences between the distribution of decussating bands in the mesial and distal loops of the anterior fold. In the distal loop, bands formed by decussating prisms are thicker than those formed by vertical prisms (Fig. $2A_2$), while in the mesial loop the reverse is observed (Fig. $2A_3$); in addition, the enamel is thicker in the distal loop, and MRE is distributed in a greater proportion (Fig. 6I, K; SOM 2: table 1). These findings may point to the direction of chewing forces, possibly indicating leading (distal loop) and trailing (mesial loop) edges in upper and lower molars.

In *Toxodon*, when present, prisms of RE are distributed radially to the EDJ in the more peripheral enamel zone, close to the outer enamel surface. This enamel type is usually related to resistance to abrasive forces, especially when opposite occlusal surfaces slide over each other, and is effective in maintaining sharp cutting surfaces, as previously proposed by Koenigswald and Sander (1997b) for rodents. The biomechanical properties of RE are evidenced, for example, in the incisors, in which there is an increased percentage of this type of enamel in the cuspal area, a condition that is possibly related to structural stress resistance. In some areas of the I2, RE occupies the highest percentage of enamel, possibly due to overload during chewing on this incisor, which usually exhibits intense wear on the internal portion of the lateral surface. Upper and lower incisors, premolars and molars show varying relative contributions of RE and MRE, with the greatest thickness of RE in areas that were probably on the push side of the cutting edges, since this enamel type is more resistant to abrasion than others, as proposed by Koenigswald et al. (1994) and Koenigswald (1997) for caviomorph rodents. In some areas of the i3, for example, where HSB reaches the outer enamel surface, RE is absent, suggesting a less intense abrasion effect. The lower premolar is conspicuous because it exhibits the thickest RE and greatest thickness of enamel on the buccal side when compared to the other cheek teeth (Fig. 6C), which could indicate intense abrasive effects on this tooth during mastication.

The enamel-dentine junction in *Toxodon* sp. is scalloped in all tooth categories analysed, consisting of raised

ridges with varying sizes, shapes, and distribution. The convexities of the scallops directed towards the dentine are characterized by a series of ridges, which look like small undulations or depressions on the dentine surface. Larger and more pronounced scallops are observed in I2, i3, p4, and the enamel folds of the upper and lower molars. Although there is controversy about the importance of the EDJ in functional interpretations, the findings observed in *Toxodon* corroborate studies that propose a relationship between scallop formation, prism decussation, and masticatory loads, with the EDJ constituting an advantageous mechanism that guards against delamination of enamel from the dentine core during mastication, without the need for further structural reinforcement, in human and non-human primates (Shimizu and Macho 2007; Brauer et al. 2010). Skinner et al. (2008) and Zhang et al. (2014) proposed a close morphological correspondence between the shape of the EDJ and the complexity of occlusal enamel in the outer enamel surface of extant and fossil primates. However, Oliveira et al. (2001) stated that the topography of the EDJ does not relate to masticatory forces, or to feeding habitats, based on microstructural analyses in diverse mammalian species.

Of note among the microstructural features observed in the upper and lower deciduous premolars of *Toxodon* is the presence of a neonatal line (NNL; Fig. 4B, C_2), a finding that is the first record in fossil mammals, with the exception of human and non-human primates. The NNL is an optical phenomenon related to alterations in the height and degree of mineralization of the enamel prisms. According to Sabel et al. (2008), the factors responsible for the development and appearance of this defect in dental hard tissues still need to be more precisely understood. However, it seems to be generally associated with physiological upset in the cellular activity of ameloblasts at birth, resulting in the formation of an accentuated incremental line, and is commonly found in fully developed deciduous premolar teeth and the developing permanent first molars (e.g., Sabel et al. 2008; Janardhanan et al. 2011; Hurnanen et al. 2019).

In the studied deciduous premolars of *Toxodon*, the NNL is almost parallel to the EDJ, with a "staircase" defect pattern, a microstructural change similar to that associated with a physiological perturbation arising from a stressor directly related to the time of birth seen in various studies on human deciduous teeth (e.g., Weber and Eisenmann 1971; Whittaker and Richards 1978; Sabel et al. 2008). The occurrence of microstructural changes associated with macroscopic enamel defects in the permanent teeth of *Toxodon* had already been presented by Braunn et al. (2014). According to these authors, hypoplastic defects were characterized by a reduction in the enamel thickness, resulting from a disruption of ameloblast activity due to systemic physiological stress that was probably related to the continuous growth of euhypsodont teeth.

The absence of HSB is observed on the lingual enamel folds of the upper and lower deciduous premolars of *Toxodon*, while on the buccal surface of these teeth there is a well-marked decussation of prisms and differentiation of enamel layers. Upper and lower deciduous premolars exhibit weakly developed HSB. These findings corroborate previous studies about the enamel features at birth in humans, indicating that deciduous tooth germs are incomplete and the enamel is only partially mineralized, as proposed by Janardhanan et al. (2011) and Hurnanen et al. (2019).

Besides the microstructural enamel features of *Toxodon* presented here, other important aspects throughout the evolutionary history of Notoungulata need to be considered with regard to dental developmental, and ontogenetic implications. From a generalized pattern with complete dentition, lack of a diastema and brachydont premolars and molars, notoungulates display a trend towards a specialized masticatory apparatus, with the emergence of euhypsodont-toothed forms with hypertrophied incisors and simplified occlusal crown patterns (e.g., Simpson 1967; Cifelli 1985; Reguero et al. 2010). Thus, a simplification of the cusps on the occlusal surface of the upper and lower cheek teeth may be associated with an increase in dental growth rates in more derived taxa. In addition to that, in "advanced" toxodontids there is evidence of a reduction or loss of the fold of the lingual enamel and fossettes/fossettids, both in the upper and lower molars (for further discussion about developmental, evolutionary, and palaeoecological implications, see, for example, Pascual 2006; Koenigswald 2011; Woodburne et al. 2014; Madden 2015; Braunn and Ribeiro 2017; Croft et al. 2020 and references therein).

It is also possible to observe changes in the types of enamel microstructure within toxodonts, with more derived features in protohypsodont and euhypsodont forms (Lindenau 2005; Madden 2015; Fillippo et. al 2019), indicating functional adaptation and the provision of greater resistance to abrasion related to the consumption of more abrasive vegetation (e.g., Simpson 1967; Janis and Fortelius 1988; Pascual and Ortiz-Jaureguizar 1990; Strömberg et al. 2013; Cassini et al. 2017).

Concerning the enamel microstructural findings presented in this study for *Toxodon* sp., it is necessary to consider the possibility that the differentiation of Schmelzmuster proposed as points of occlusion produced during masticatory loading of the teeth may actually correspond to primitive contacts between cusps that were in occlusion in the ancestral species, which persisted through changes in cheek tooth pattern, and may thus constitute an example of ancestral trait retention.

Since tooth wear patterns at both the macro- and microscopic levels may have been influenced during the evolution of the teeth by a need to reduce high tensile stresses (Ungar 2015), the morphology of the dental axis could have been selected to maintain chewing efficiency throughout the life of these euhypsodont animals, as was proposed by Benazzi et al. (2013a, b) for human teeth. From this it is possible to infer that the behaviour of ameloblasts forming enamel prisms during amelogenesis is guided by genetic/evolution-

ary controls that act to increase the fracture and wear resistance of tooth enamel, as was proposed by Lynch et al. (2010). For these reasons, features such as the topography of the occlusal surface in relation to the dental axis, functional biomechanics, enamel thickness, and microstructural organization should be considered in response to occlusal load (Benazzi et al. 2013a, b).

Conclusions

The microstructural data presented here indicate that the evolution of the dental morphology of Notoungulata related to hypsodonty was accompanied by correlated enamel microstructural changes. The spatial relationships between the enamel types may, as observed here in *Toxodon* sp., indicate that the greater percentage of HSB implies a functional adaptation to provide a greater resistance to the consumption of more abrasive vegetation. Incisors, premolars, and molars show different proportions of enamel types that contribute to the total enamel thickness in each tooth category. Upper and lower permanent and deciduous premolars exhibit differentiation of the Schmelzmuster on the buccal and lingual sides of the dental axis, which is dependent on the tooth series and location within it; these findings are possibly related to biomechanical, evolutionary, and palaeoecological demands. Comparative analyses allowed the recognition of differences between the lingual enamel folds of the upper and lower molars of *Toxodon* sp. with regards to the proportions of the layers of this tissue, which could have a functional significance, indicating leading and trailing microstructural features in these teeth.

Acknowledgements

For the assistance with the histologic sections we thank João Bonaldo (Universidade Federal de Pelotas, Pelotas, Brazil). Thanks also to Deise Henriques (Museu Nacional, Universidade Federal do Rio de Janeiro, Rio de Janeiro, Brazil) and Jamil Pereira (Museu Coronel Tancredo Fernandes de Mello, Santa Vitória do Palmar, Brazil), for facilitate the study of specimens of *Toxodon*, some of them for histological studies. We thank the APP Editor Olivier Lambert (Royal Belgian Institute of Natural Sciences, Brussels, Belgium), as well as the reviewers Agustín Martinelli (Museo Argentino de Ciencias Naturales Bernardino Rivadavia, Buenos Aires, Argentina) and Tomaz Melo (Universidade Federal do Rio Grande do Sul, Porto Alegre, Brazil), for their valuable suggestions and corrections that greatly enhanced this work. For the grammatical review, we thank Katarzina Piper (Bere Alston, UK). We thank the Centro de Microscopia e Microanálise of Universidade Federal do Rio Grande do Sul for help during imaging of specimens, the Conselho Nacional de Desenvolvimento Científico e Tecnológico for financial support to PRB during her study at the PPG Geociências/UFRGS (CNPq 140736/2012-3) and AMR (CNPq 312085/2013-3 and 306951/2017-7), the Museu de Ciências Naturais/SEMA-RS (Brazil) for the infrastructure provided, Karen Adami for allowing the use of the Laboratory of Mineralogy of the Universidade Federal de Pelotas, and Luiz Rota (Santa Vitória do Palmar, Brazil), for collecting fossil specimens from this study.

References

Alloing-Séguier, L., Lihoreau, F., Boisserie, J.-R., Charruault, A.-L., Orliac, M., and Tabuce, R. 2014. Enamel microstructure evolution in anthracotheres (Mammalia, Cetartiodactyla) and new insights on hippopotamoid phylogeny. *Zoological Journal of the Linnean Society* 171: 668–695.

Bauzá, N., Gelfo, J.N., and López, G.M. 2019. Early steps in the radiation of notoungulate mammals in southern South America: A new henricosborniid from the Eocene of Patagonia. *Acta Palaeontologica Polonica* 64: 597–603.

Benazzi, S., Nguyen, H.N., Kullmer, O., and Hublin, J. 2013a. Unravelling the functional biomechanics of dental features and tooth wear. *PLoS ONE* 8: e69990.

Benazzi, S., Nguyen, H.N., Schulz, D., Grosse, I.R., Gruppioni G., Hublin, J., and Kullmer, O. 2013b. The evolutionary paradox of tooth wear: simply destruction or inevitable adaptation? *PLoS ONE* 8: e62263.

Bergqvist, L.P. and Koenigswald, W. von 2017. The dentition of *Carodnia vieirai* (Mammalia: Xenungulata): Enamel microstructure and mastication pattern. *Palaeontologia Electronica* 20.2.30A: 1–15.

Billet, G. 2011. Phylogeny of the Notoungulata (Mammalia) based on cranial and dental characters. *Journal of Systematic Palaeontology* 9: 481–497.

Bond, M. 1986. Los ungulados fósiles de Argentina: Evolución y paleoambientes. *In*: A.J. Cuerda, J.F. Bonaparte, W., Volkheimer, and H.A. Leanza (orgs.), *Actas del IV Congreso Argentino de Paleontología y Bioestratigrafia, Mendoza, 23–27 November 1986*, 173–185. Asociación Paleontológica Argentina, Mendoza.

Bond, M. 1999. Quaternary native ungulates of Southern South America. A synthesis. *In:* J. Rabassa and M. Salemme (eds.), *Quaternary of South America and Antarctic Peninsula* 12: 177–205.

Bond, M., Cerdeño, E., and López, G. 1995. Los ungulados nativos de América del Sur. *In*: M.T. Alberdi, G. Leone, and E.P. Tonni (eds.), *Evolución biológica y climática de la región pampeana durante los últimos cinco millones de años. Un ensayo de correlación con el Mediterráneo occidental, Monografías del Museo Nacional de Ciencias Naturales 12*, 259–275. Consejo Superior de Investigaciones Científicas, Madrid.

Boyde, A. and Fortelius, M. 1986. Development, structure and function of rhinoceros enamel. *Zoological Journal of Linnean Society* 87: 181–214.

Brauer, D.S., Marshall, G.W., and Marshall, S.J. 2010. Variations in human DEJ scallop size with tooth type. *Journal of Dentistry* 38: 597–601.

Braunn, P.R. and Ribeiro, A.M. 2017. Evolução dos Toxodontia da América do Sul durante o Cenozoico: aspectos dentários, paleoclimáticos e paleoambientais. *Terræ Didatica* 13: 127–145.

Braunn, P.R., Ribeiro, A.M., and Ferigolo, J. 2014. Microstructural defects and enamel hypoplasia in teeth of *Toxodon* Owen, 1837 from the Pleistocene of southern Brazil. *Lethaia* 47: 418–431.

Carlini, A.A. and Tonni, E.P. 2000. *Mamíferos Fósiles del Paraguay*. 108 pp. Cooperación Técnica Paraguayo-Alemana, Proyecto Sistema Ambiental del Chaco, Proyecto Sistema Región Oriental, Buenos Aires.

Cassini, G.H., Del Pino, S.H., Munõz, N.A., Acosta, W.G., Fernández, M., Bargo, M.S., and Vizcaíno, S.F. 2017. Teeth complexity, hypsodonty and body mass in Santacrucian (Early Miocene) notoungulates (Mammalia). *Earth and Environmental Science Transactions of the Royal Society of Edinburgh* 106: 303–313.

Chai, H., Lee, J.J., Constantino, P.J., Lucas, P.W., and Lawn, B.R. 2009. Remarkable resilience of teeth. *Proceedings of the National of Sciences of the United States of America* 106: 7289–7293.

Cifelli, R.L. 1985. South American Ungulate Evolution and Extinction. *In*: S.D. Webb (ed.), *The Great American Biotic Interchange*, 249–266. Plenum Press, New York.

Cifelli, R.L. 1993. The phylogeny of the South American ungulates. *In*: F.S. Szalay, M.J. Novacek, and M.C. McKenna (eds.), *Mammal Phylogeny: Placentals, 2*, 195–216. Springer-Verlag, New York.

Croft, D.A., Gelfo, J.N., and López, G.M. 2020. Splendid Innovation: the extinct South American native ungulates. *Annual Review of Earth and Planetary Sciences* 48: 259–290.

Darwin, C. 1845. *Journal of Researches into the Natural History and Geology of the Countries Visited during the Voyage of HMS Beagle round the World, under the Command of Captain Fitzroy*. 279 pp. John Murray, London.

Elissamburu, A. 2012. Estimación de la masa corporal en géneros del Orden Notoungulata. *Estudios Geológicos* 68: 91–111.

Ferretti, M.P. 1999. Tooth enamel structure in the hyaenid *Chasmaporthetes lunensis* from the Late Pliocene of Italy, with implications to feeding behavior. *Journal of Vertebrate Paleontology* 19: 767–770.

Fillippo, A., Kalthoff, D.C., Billet, G., and Rodrigues, H.G. 2020. Evolutionary and functional implications of incisor enamel microstructure diversity in Notoungulata (Placentalia, Mammalia). *Journal of Mammal Evolution* 27: 211–236.

Fortelius, M. 1985. Ungulate cheek teeth: developmental, functional, and interrelations. *Acta Zoologica Fennica* 180: 1–76.

Guérin, C. and Faure, M. 2013. Un nouveau Toxodontidae (Mammalia, Notoungulata) du Pléistocène supérieur du Nordeste du Brésil. *Geodiversitas* 35: 155–205.

Guidón, N., Parenti, F., Da Luz, M.F., Guérin, C., and Faure, M. 1994. Le plus ancien peuplement de L'Amérique: le Paléolithique du nordeste brésilien. *Bulletin de la Société préhistorique française* 91: 246–250.

Hoffstetter, R. 1978. Une faune de Mammifères pléistocènes au Paraguay. *Comptes Rendus Sommaires des Sciences de la Société Géologique de France* 1978: 32–33.

Hurnanen, J., Sillanpää, M., Mattila, M.L., Löyttyniemi, E., Witzel, C., and Rautava, J. 2019. Staircase-pattern neonatal line in human deciduous teeth is associated with tooth type. *Archives of Oral Biology* 104: 1–6.

Janardhanan, J.M., Umadethan, B., Biniraj, K.R., Vinod Kumar, R.B., and Rakesh, S. 2011. Neonatal line as a linear evidence of live birth: Estimation of postnatal survival of a new born from primary tooth germs. *Journal of Forensic Dental Sciences* 3: 8–13.

Janis, C.M. and Fortelius, M. 1988. On the means whereby mammals achieve increased functional durability of their dentitions, with special reference to limiting factors. *Biological Reviews* 63: 197–230.

Kawai, N. 1955. Comparative anatomy of bands of Schreger. *Okajimas Folia Anatomica Japonica* 27: 115–131.

Koenigswald, W. von 1988. Enamel modification in enlarged front teeth among mammals and the various possible reinforcement of the enamel. *In*: D.E. Russell, J.-P. Santoro, and D. Sigogneau-Russell (eds.), Teeth Revisited: Proceedings of the VIIth International Symposium on Dental Morphology, Paris 1986. *Mémoires du Muséum National d'Histoire Naturelle, Paris (série C)* 53: 147–167.

Koenigswald, W. von 1992. Tooth enamel of the cave bear (*Ursus spelaeus*) and the relationship between diet and enamel structures. *Annales Zoologici Fennici* 28: 217–227.

Koenigswald, W. von 1997. Brief survey of enamel diversity at the Schmelzmuster level in Cenozoic placental mammals. *In*: W. von Koenigswald and P.M. Sander (eds.), *Tooth Enamel Microstructure*, 137–161. A.A. Balkema, Rotterdam.

Koenigswald, W. von 2011. Diversity of hypsodont teeth in mammalian dentitions—construction and classification. *Palaeontographica A: Palaeozoology Stratigraphy* 294: 63–94.

Koenigswald, W. von and Clemens, W.A. 1992. Levels of complexity in the microstructure of mammalian enamel and their application in studies of systematics. *Scanning Microscopy* 6: 195–218.

Koenigswald, W. von and Krause, D.W. 2014. Enamel microstructure of *Vintana sertichi* (Mammalia, Gondwanatheria) from the Late Cretaceous of Madagascar. *Journal of Vertebrate Paleontology* 34: 166–181.

Koenigswald, W. von and Sander, P.M. 1997a. Glossary of terms used for enamel microstructures. *In*: W. von Koenigswald and P.M. Sander (eds.), *Tooth Enamel Microstructure*, 267–280. A.A. Balkema, Rotterdam.

Koenigswald, W. von and Sander, P.M. 1997b. Schmelzmuster differentiation in leading and trailing edges, a specific biomechanical adaptation in rodents. *In*: W. von Koenigswald and P.M. Sander (eds.), *Tooth Enamel Microstructure*, 259–266. A.A. Balkema, Rotterdam.

Koenigswald, W. von, Holbrook, L.T., and Rose, K.D. 2011. Diversity and evolution of Hunter-Schreger Band configuration in tooth enamel of perissodactyl mammals. *Acta Palaeontologica Polonica* 56: 11–32.

Koenigswald, W. von, Rensberger, J.M., and Pfretzschner, H. 1987. Changes in the tooth enamel of early Paleocene mammals allowing increased diet diversity. *Nature* 328: 150–152.

Koenigswald, W. von, Sander, P.M., Leite, M., Mörs, M., and Santel, W. 1994. Functional symmetries in the Schmelzmuster and morphology in rootless rodent molars. *Zoological Journal of the Linnean Society* 110: 141–179.

Lindenau, C. 2005. *Zahnschmelzmikrostrukturen Südamerikanischer Huftiere*. 245 pp. Ph.D. dissertation, Universität Bonn, Bonn.

Line, S.R.P. and Bergqvist, L.P. 2005. Enamel structure of Paleocene mammals of the São José de Itaboraí Basin, Brazil. 'Condylarthra', Litopterna, Notoungulata, Xenungulata, and Astrapotheria. *Journal of Vertebrate Paleontology* 25: 924–928.

Lucas, P., Constantino, P., Wood, B., and Lawn, B. 2008. Dental enamel as a dietary indicator in mammals. *BioEssays* 30: 374–385.

Lundelius Jr., E.L., Bryant, V.M., Mandel, R.D., and Thoms, A. 2013. The first occurrence of a toxodont (Mammalia, Notoungulata) in the United States. *Journal of Vertebrate Paleontology* 33: 229–232.

Lynch, C.D., O'Sullivan, V.R., Dockery, P., McGillycuddy, C.T., and Sloan, A.J. 2010. Hunter-Schreger band patterns in human tooth enamel. *Journal of Anatomy* 217: 106–115.

Maas, M.C. 1994. A scanning electron microscopic study of in vitro abrasion of mammalian tooth enamel under compressive loads. *Archives of Oral Biology* 39: 1–11.

Maas, M.C. 1997. Enamel microstructure in notoungulates. *In*: R.F. Kay., R.H. Madden, R.L. Cifelli, and J.J. Flynn (eds.), *Vertebrate Paleontology in the Neotropics: the Miocene Fauna of La Venta, Colombia*, 319–334. Smithsonian Institution Press, Washington DC.

Maas, M.C. and Thewissen, J.G.M. 1995. Enamel microstructure of *Pakicetus* (Mammalia: Archaeoceti). *Journal of Vertebrate Paleontology* 69: 1154–1163.

Madden, R.H. 1997. A new toxodontid notoungulate. *In*: R.F. Kay., R.H. Madden, R.L. Cifelli, and J.J. Flynn (eds.), *Vertebrate Paleontology in the Neotropics: the Miocene Fauna of La Venta, Colombia*, 335–354. Smithsonian Institution Press, Washington DC.

Madden, R.H. 2015. *Hypsodonty in Mammals*. *Evolution, Geomorphology, and the Role of Earth Surface Processes*. 446 pp. Cambridge University Press, Cambridge.

Marshall, L.G., Berta, A.R., Hoffstetter, R., Pascual, R., Reig, O., Bombin, M., and Mones, A. 1984. Mammals and stratigraphy: geochronology of the continental mammal-bearing Quaternary of South America. *Palaeovertebrata Mémoire Extraordinaire, Montpellier* 14: 1–76.

Oliveira, C.A., Bergqvist, L.P., and Line, S.R.P. 2001. A comparative analysis of the structure of the dentinoenamel junction in mammals. *Journal of Oral Science* 43: 277–281.

Owen, R. 1837. A description of the cranium of the *Toxodon platensis*, a gigantic extinct mammiferous species, referible by its dentition to the Rodentia, but with affinities to the Pachydermata and the herbivorous Cetacea. *Geological Society of London, Proceedings* 2: 541–542.

Pascual, R. 2006. Evolution and geography: the biogeographic history of South American land mammals. *Annals of the Missouri Botanical Garden* 93: 209–230.

Pascual, R. and Ortiz-Jaureguizar, E. 1990. Evolving climates and mammal faunas in Cenozoic South America. *Journal of Human Evolution* 19: 23–60.

Paula-Couto, C. 1979. *Tratado de Paleomastozoologia*. 590 pp. Academia Brasileira de Ciências, Rio de Janeiro.

Pfretzschner, H. 1988. Structural reinforcement and crack propagation in enamel. *In*: D.E. Russell, J.-P. Santoro, and D. Sigogneau-Russell (eds.), Teeth Revisited: Proceedings of the VIIth International Symposium on Dental Morphology, Paris 1986. *Mémoires du Muséum National d'Histoire Naturelle, Paris (série C)* 53: 133–143.

Pfretzschner, H. 1992. Enamel microstructure and hypsodonty in large mammals. *In*: P. Smith and E. Tchernov (eds.), *Structure, Function and Evolution of Teeth*, 147–162. Freund Publishing House, London.

Pfretzschner, H. 1994. Biomechanik der Schmelzmikrostruktur in den Backenzähnen von Grossägern. *Palaeontographica A* 234: 1–88.

Politis, G.G. and Gutiérrez, M. 1998. Gliptodontes y Cazadores-Recolectores de la Región Pampeana (Argentina). *Latin American Antiquity* 9: 111–134.

Politis, G.G., Gutiérrez, M., Rafuse, D.J., and Blasi, A. 2016. The arrival of *Homo sapiens* into the Southern Cone at 14,000 Years Ago. *PLoS ONE* 11: e0162870.

Popowics, T.E, Rensberger, J.M., and Herring, S.W. 2001. The fracture behaviour of human and pig molar cusps. *Archives of Oral Biology* 46: 1–12.

Reguero, M.A., Candela, A.M., and Cassini, G.H. 2010. Hypsodonty and body size in rodent-like notoungulates. *In*: R. Madden, A.A. Carlini, M.G. Vucetich, and R. Kay (eds.), *The Paleontology of Gran Barranca: Evolution and Environmental Change through the Middle Cenozoic of Patagonia*, 362–371. Cambridge University Press, Cambridge.

Rensberger, J.M. 1995. Determination of stresses in mammalian dental enamel and their relevance to the interpretation of feeding behaviours in extinct taxa. *In*: J. Thomason (ed.), *Functional Morphology in Vertebrate Paleontology*, 151–172, Cambridge University Press, Cambridge.

Rensberger, J.M. 1997. Mechanical adaptation in enamel. *In*: W. von Koenigswald and P.M. Sander (eds.), *Tooth Enamel Microstructure*, 237–257. A.A. Balkema, Rotterdam.

Rensberger, J.M. 2000. Pathways to functional differentiation in mammalian enamel. *In*: M.F. Teaford, M.M. Smith, and M.W.J. Ferguson (eds.), *Development Function and Evolution of Teeth*, 252–268. Cambridge University Press, Cambridge.

Rensberger, J.M. and Koenigswald, W. von 1980. Functional and phylogenetic interpretation of enamel microstructure in rhinoceroses. *Paleobiology* 6: 477–495.

Sabel, N., Johansson, C., Kühnisch, J., Robertson, A., Steiniger, F., Norén, J.G., Klingberg, G., and Nietzsche, S. 2008. Neonatal lines in the enamel of primary teeth—a morphological and scanning electron microscopic investigation. *Archives of Oral Biology* 53: 954–963.

Shimizu, D. and Macho, G.A. 2007. Functional significance of the microstructural detail of the primate dentino-enamel junction: a possible example of exaptation. *Journal of Human Evolution* 52: 103–111.

Shimizu, D., Macho, G.A., and Spears, I.R. 2005. Effect of prism orientation and loading direction on contact stresses in prismatic enamel of primates: implications for interpreting wear patterns. *American Journal of Physical Anthropology* 126: 427–434.

Simpson, G.G. 1967. The beginning of the age of mammals in South America. Part 2, Systematics: Notoungulata, concluded (Typotheria, Hegetotheria, Toxodonta, Notoungulata *incertae sedis*), Astrapotheria, Trigonostylopoidea, Pyrotheria, Xenungulata, Mammalia *incertae sedis*. *Bulletin of the American Museum of Natural History* 137: 1–259.

Skinner, M.M., Wood, B.A., Boesch, C., Olejniczak, A.J., Rosas, A., Smith, T.M., and Hublin, J.J. 2008. Dental trait expression at the enamel-dentine junction of lower molars in extant and fossil hominoids. *Journal of Human Evolution* 54: 173–186.

Steffen, C. 1999. Enamel microstructure of recent and fossil Canidae (Carnivora: Mammalia). *Journal of Vertebrate Paleontology* 19: 576–587.

Steffen, C. 2001. Enamel structure of arctoid Carnivora: Amphicyonidae, Ursidae, Procyonidae, and Mustelidae. *Journal of Mammalogy* 82: 450–462.

Strömberg, C.A., Dunn, R.E., Madden, R.H., Kohn, M.J., and Carlini, A.A. 2013. Decoupling the spread of grasslands from the evolution of grazer-type herbivores in South America. *Nature Communications* 4: 1–8.

Tabuce, R., Delmer, C., and Gheerbrant, E. 2007. Evolution of the tooth enamel microstructure in the earliest proboscideans (Mammalia). *Zoological Journal of the Linnean Society* 179: 611–628.

Tonni, E.P., Alberdi, M.T., Prado, J.L., Bargo, M.S., and Cione, A.L. 1992. Changes on mammal assemblages in the Pampean region (Argentina) and their relation with the Plio-Pleistocene boundary. *Palaeogeography, Palaeoclimatology, Palaeoecology* 95: 179–194.

Ungar, P.S. 2015. Mammalian dental function and wear: A review. *Biosurface and Biotribology* 1: 25–41.

Van Frank, R. 1957. A fossil collection from northern Venezuela 1. Toxodontidae (Mammalia, Notoungulata). *American Museum Novitates* 18: 1–38.

Vieytes, E.C., Morgan, C.C., and Verzi, D.H. 2007. Adaptive diversity of incisor enamel microstructure in South American burrowing rodents (family Ctenomyidae, Caviomorpha). *Journal of Anatomy* 211: 296–302.

Weber, D.F. and Eisenmann, D.R. 1971. Microscopy of the neonatal line in developing human enamel. *The American Journal of Anatomy* 141: 375–391.

Whittaker, D.K. and Richards, D. 1978. Scanning electron microscopy of the neonatal line in human enamel. *Archives of Oral Biology* 23: 45–50.

Wood, C.B., Dumont, E.R., and Crompton, A.W. 1999. A review of enamel microstructure in non therian mammals: implications for enamel prisms as a synapomorphy of Mammalia. *Journal of Mammalian Evolution* 6: 177–214.

Woodburne, M.O., Goin, F.J., Bond, M., Carlini, A.A., Gelfo, J.N., López, G.M., Iglesias, A., and Zimicz, A.N. 2014. Paleogene land mammal faunas of South America; a response to global climatic changes and indigenous floral diversity. *Journal of Mammalian Evolution* 21: 1–73.

Zhang, Y., Kono, R.T., Jin, C., Wang, W., and Harrison, T. 2014. Possible change in dental morphology in *Gigantopithecus blacki* just prior to its extinction: evidence from the upper premolar enamel-dentine junction. *Journal of Human Evolution* 75: 166–171.

Zimicz, A.N., Fernández, M., Bond, M., Chornogubsky, L., Arnal, M., Cárdenas, M., and Fernicola, J.C. 2020. *Archaeogaia macachaae* gen. et sp. nov., one of the oldest Notoungulata Roth, 1903 from the early–middle Paleocene Mealla Formation (Central Andes, Argentina) with insights into the Paleocene–Eocene south American biochronology. *Journal of South American Earth Sciences* 103. [published online, https://doi.org/10.1016/j.jsames.2020.102772]